IEEE Access
Multidisciplinary | Rapid Review | Open Access Journal

Received March 8, 2018, accepted April 11, 2018, date of publication April 17, 2018, date of current version May 9, 2018.

Digital Object Identifier 10.1109/ACCESS.2018.2828043

Transient Behavior Analysis of Offshore Wind Turbines During Lightning Strike to Multi-Blade

SHIQI TAO, XIAOQING ZHANG, YAOWU WANG, AND JUNFENG YANG
School of Electrical Engineering, Beijing Jiaotong University, Beijing 100044, China

Corresponding author: Shiqi Tao (13121467@bjtu.edu.cn)

This work was supported in part by the National Natural Science Foundation of China under Grant 51420105011 and in part by the Fundamental Research Funds for the Central Universities under Grant E17JB00180.

ABSTRACT A set of analytic formulas are presented to evaluate the circuit parameters of blade, tower, three-phase cable, and monopile foundation. On the basis of the circuit parameters, the circuit model is built and a transient analysis is carried out for the offshore wind turbine (WT) under lightning strikes to multi-blade. The lightning transient responses can be obtained at the different locations of the offshore WT by using the circuit model. An experimental measurement with a reduced-scale WT has been made for checking the validity of the circuit parameter formulas and circuit model. The measured results are compared with the calculated ones and a good agreement is shown between them. The practical feasibility of the circuit model is also examined by a numerical example of an actual Chinese-built offshore WT.

INDEX TERMS Lightning, offshore wind turbine, circuit model, transient response, reduced-scale experiment.

I. INTRODUCTION

Wind turbines (WTs) are especially susceptible to lightning strikes due to their height, distinctive shape and exposed location. According to field observations, WTs experience a significant number of lightning strikes during their lifetime [1], mostly to the blades. The lightning current causes severe damages that involve considerable costs of repair-materials, labor, and downtime to the blade structural materials. According to the statistical data reported in [2], about 4%-8% wind turbines have been damaged by lightning in Denmark, Sweden and Germany each year. In recent years, the serious lightning accidents often appear in Hainan East Wind Farm in China, the damage rate of blades amounts to 5.56% [3]. In actual cases, lightning flash is likely to strike not only single-blade but also multi-blade. Although the inspections at the offshore wind farms are carried out after thunderstorms, it is difficult to determine with certainty the cause of every damaged blade. The possible mechanisms for lightning strike to multi-blade include: 1. A single lightning sweeps from one blade to another due to the blades rotation; 2. Different branches of a single lightning strike are attached to the blades; 3. Subsequent lightning strikes are attached to the blades. Despite the fact that the probability of lightning strike to multi-blade is relatively small, the blades damage and economic loss are larger than those under the lightning strike to single-blade [4].

As far as the lightning transient analysis of the offshore WT is concerned, the existing works mainly focus on lightning strike to single-blade [5], [6], whereas few researches involve lightning strike to multi-blade. This leads to a deficiency that a special consideration of lightning strike to multi-blade has not been given in the design of lightning protection [7]–[10]. Therefore, a lightning transient analysis of offshore WTs is made in this paper with a special concern to lightning strike to multi-blade. The circuit parameters are obtained and the equivalent circuit model is built for the offshore WTs during lightning strike to multi-blade and their validity are confirmed by the experimental measurement with reduced-scale WT. A numerical example is also given for examining the practical feasibility of the circuit model.

II. MODELING OF THE OFFSHORE WT

A. LIGHTNING CURRENTS

As the current source injected into the WT, the positive lighting current $+10/350\mu$s and negative lighting current $-1/200\mu$s are used in the transient analysis of offshore wind turbines, respectively [2]. Their current waveforms can be expressed by the double-exponential function [6]

$$i(t) = KI_m(e^{-\alpha t} - e^{-\beta t}) \tag{1}$$

where I_{m} is the peak value of lightning current and other parameters are listed in Tab. 1.

TABLE 1. Parameters of double-exponential function.

Waveforms	Fitting constants		
	K	α	β
+10/350μs	1.025	2.05×10^{3}	5.64×10^{5}
−1/200μs	1.002	3.5×10^{3}	7.78×10^{6}

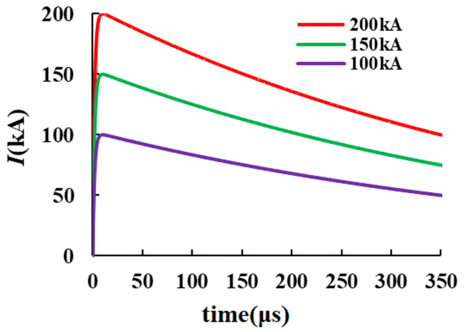

(a)

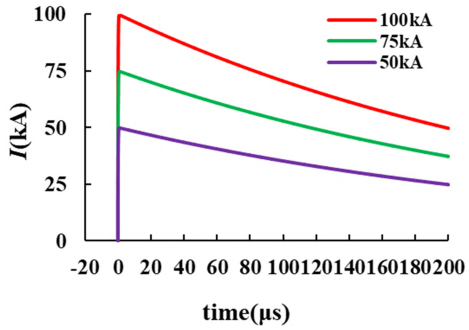

(b)

FIGURE 1. Lightning current waveforms. (a) Positive lighting current +10/350μs, (b) Negative lightning lighting current |−1/200μs|.

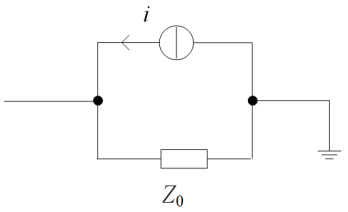

FIGURE 2. Model of injected lightning current.

Considering the multiple situations of lightning strike to blades, the peak values of $+10/350\mu$s are taken as 200kA, 150kA and 100kA, and those of $-1/200\mu$s are taken as −100kA, −75kA, −50kA according to the relevant design standard [2], [7], as shown in Fig. 1(a), (b).

The circuit representation of the current source injected the WT is given in Fig. 2, where Z_0 (300Ω∼400Ω) is the surge impedance of the lightning channel [11], [12].

B. BLADE

In general, the down conductor is installed inside the blade for conducting lightning current. To perform transient analysis, the down conductor needs to be divided into a number

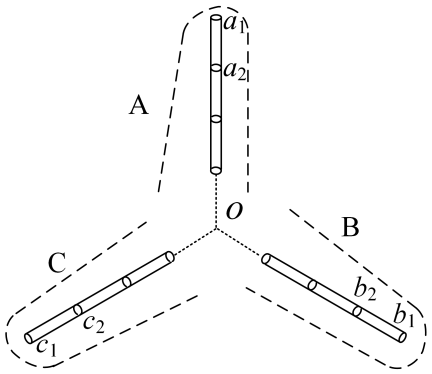

FIGURE 3. Segmentation of blades.

of segments to take account of the propagation wave phenomenon of lightning current, as shown in Fig. 3 [8]. The blade may also be described by the non-uniform transmission line model. However, owing to the complexity of the spatial conductor position, the self and mutual surge impedances are difficult to evaluate accurately.

For arbitrary segment b ($b = 1, 2 \ldots m$), its resistance is estimated as [9]:

$$R_{\mathrm{b}} = \frac{\rho l_{\mathrm{b}}}{\pi\sigma\left[\left(1-e^{(-r_{\mathrm{b}}/\sigma)}\right)\right]\left[2r_{\mathrm{b}}-\sigma\left(1-e^{(-r_{\mathrm{b}}/\sigma)}\right)\right]} \quad (2)$$

where ρ is the material resistivity, l_b is the length of each segment, r_{b} is the radius of the down-conductor. The skin depth σ is

$$\sigma = \frac{1}{\sqrt{\pi f \mu\gamma}} \quad (3)$$

where μ is the material permeability and $\gamma = 1/\rho$. The frequency f may be roughly evaluated by the waveform parameters of the injected lightning current [12], [13].

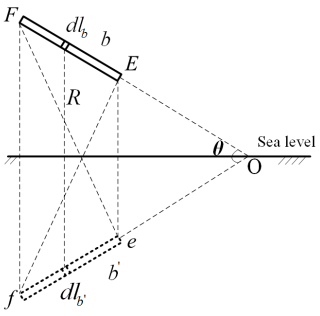

FIGURE 4. Conductor segment and its image.

The capacitance of segment b can be calculated by the average potential method [14], [15]. The sea level is regarded as an infinite perfect conductor for simplification purpose and its presence is taken into account by the image method. In Fig. 4, the image segment is depicted in dotted line. It is installed symmetrically below the sea level with respective to the real segment. According to the image symmetry,

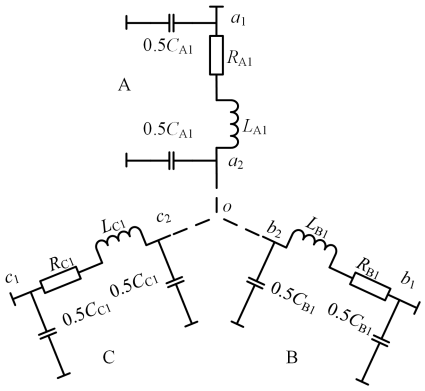

FIGURE 5. π-circuit model of three blades.

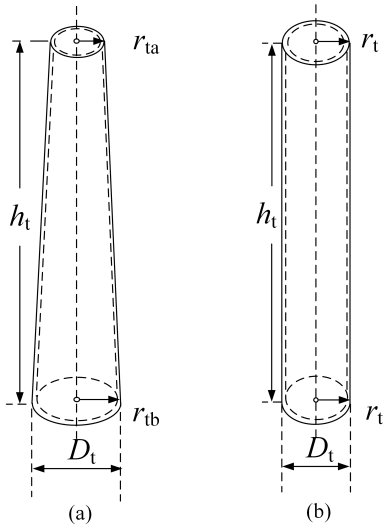

FIGURE 6. Structural simplification of tower. (a) Actual tower body, (b) Cylindrical shell.

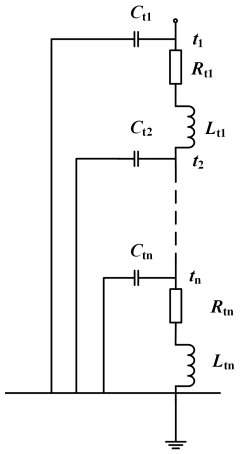

FIGURE 7. Chain-type circuit model of tower.

the length of each image segment is equal to that of its corresponding real segment.

Let τ be the linear charge density of branch conductor and ε_0 is the space permittivity. At a point on segment b,

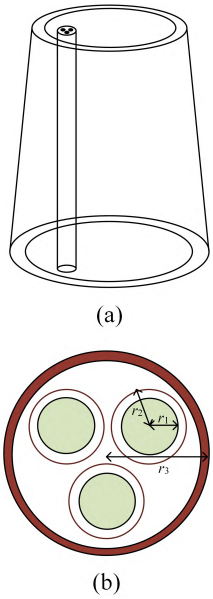

FIGURE 8. Three-phase cable. (a) Schematic diagram, (b) Cross-section drawing.

the average potential generated by its image b' is expressed by

$$\bar{u}_{bb'} = \frac{\tau}{4\pi\varepsilon_0 l_b} G_{bb'} \tag{4}$$

where

$$G_{bb'} = \int_{l_b}\int_{l_{b'}} \frac{1}{R} dl_{b'} dl_b \tag{5}$$

Calculation of the average potential coefficient includes an evaluation of the double integrals $G_{bb'}$. This integral depends on the relative positions between their respective integral paths, as shown in Fig. 4. Through complicated integral operation, $G_{bb'}$ is given by:

$$\begin{aligned} G_{bb'} = [&(\alpha + l_b)\ln\frac{D_1 + D_2 + l_b}{D_1 + D_2 - l_b} - \alpha\ln\frac{D_3 + D_4 + l_b}{D_3 + D_4 - l_b} \\ &+ (\beta + l_b)\ln\frac{D_1 + D_4 + l_b}{D_1 + D_4 - l_b} - \beta\ln\frac{D_2 + D_3 + l_b}{D_2 + D_3 - l_b}] \end{aligned} \tag{6}$$

where α and β are the lengths of OE and Oe, D_1, D_2, D_3 and D_4 are the length of Ff, Fe, Ee, and Ef, respectively. Similarly, the average potential $\bar{u}_{bb}$ is expressed by [16]

$$\begin{aligned} \bar{u}_{bb} &= \frac{\tau}{4\pi\varepsilon_0 l_b} G_{bb} \\ &= \frac{\tau}{4\pi\varepsilon_0 l_b}\left[2l_b\ln\left(\frac{r_b}{\sqrt{l_b^2 + r_b^2} - l_b}\right)\right. \\ &\quad \left. + 2\left(r_b - \sqrt{l_b^2 + r_b^2}\right)\right] \end{aligned} \tag{7}$$

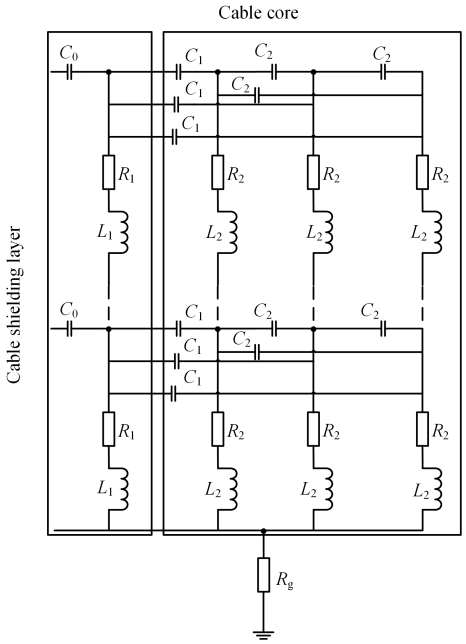

FIGURE 9. Circuit model of three-phase cable.

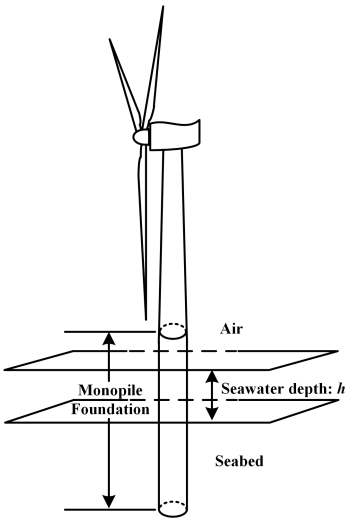

FIGURE 10. Schematic diagram of an offshore WT.

By using the integral formulas given above, the capacitance of the segment b is given by

$$C_{\mathrm{b}} = \frac{\tau l_{\mathrm{b}}}{\bar{u}_{\mathrm{bb}} - \bar{u}_{\mathrm{bb}'}} = \frac{4\pi\varepsilon_0 l_{\mathrm{b}}^2}{G_{\mathrm{bb}} - G_{\mathrm{bb}'}} \tag{8}$$

In terms of G_{bb} and $G_{\mathrm{bb}'}$, the inductance L_{b} of segment b is also calculated by the Neumann's integral formula [17], [18]

$$L_{\mathrm{b}} = \frac{\mu_0}{4\pi}\left(G_{\mathrm{bb}} - G_{\mathrm{bb}'}\right) \tag{9}$$

Since the electromagnetic coupling between the blade and tower is weak, the influence of the tower is ignored in the circuit parameter calculation of the blade. Based on the circuit parameters, each segment can be represented as a π-circuit, as shown in Fig. 5. The π-circuit model can take account

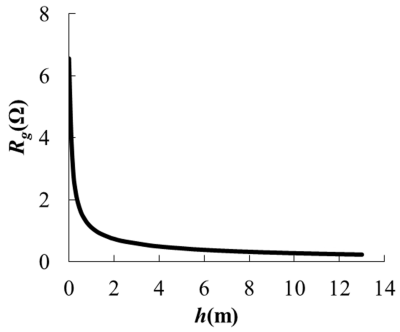

FIGURE 11. R_g-h curve. (R_g: grounding resistance; h: seawater depth).

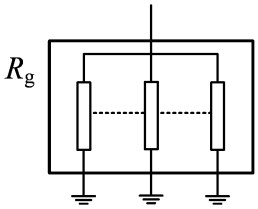

FIGURE 12. Circuit representation of grounding resistance.

FIGURE 13. Three damaged blades.

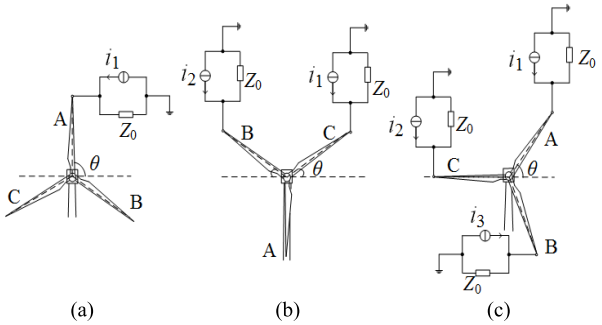

FIGURE 14. Three cases of lightning strike. (a) Single-blade, (b) Two-blade, (c) Three-blade.

of the propagation phenomenon of lightning current and also convenient to calculate the transient response at the different locations on the blade through a reasonable segmentation.

TABLE 2. Peak values of +10/350μs and −1/200μs under lightning strike to multi-blade.

Waveforms	Lightning location	Peak values of lightning current(kA)
+10/350μs	Blade A	200
	Blade B,C	150,150
	Blade A,C,B	200,150,100
−1/200μs	Blade A	−100
	Blade B,C	−75, −75
	Blade A,C,B	−100, −75, −50

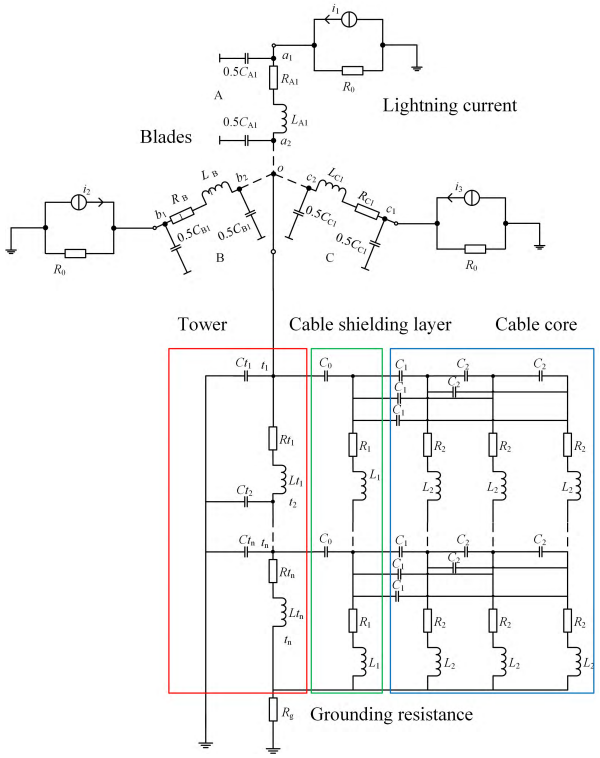

FIGURE 15. Complete equivalent circuit of a WT.

C. TOWER AND THREE-PHASE CABLE

1) TOWER

An offshore WT tower is a tubular circular truncated cone, as shown in Fig. 6(a). In actual situation, h_t is much greater than r_{ta} and r_{tb} , and there is no significant difference between r_{ta} and r_{tb}. Therefore, the tower body may be simplified as a cylindrical shell, as shown in Fig. 6(b). In consideration of propagation wave phenomenon of lightning current traveling on the tower, the continuous cylindrical shell is approximately dissected into a number of segments [19], [20].

For an arbitrary segment m ($m = 1, 2 \ldots n$), the resistance R_{tm} of segment m is estimated by (10).

$$R_{tm} = \left[1 + \left(\sqrt{\frac{q}{2}} - 1\right)\left(1 - \frac{w}{r_t} - \frac{8}{4\sqrt{2q} - 5}\left(\frac{w}{r_t}\right)^2\right)\right] R_{tm0} \tag{10}$$

where $r_t = (r_{ta} + r_{tb})/2$, $q = 2\pi f \mu\sigma\omega^2$, μ is the material permeability, ω is the thickness of tower, and R_{tm0} is the DC resistance.

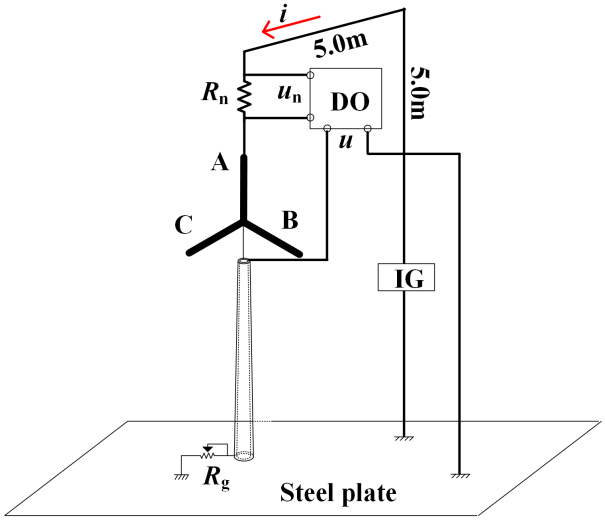

FIGURE 16. Diagram of experimental arrangement. (IG: Impulse generator; DO: Digital oscilloscope).

TABLE 3. Dimensions of the blades and tower in experimental arrangement.

Blade(mm)		Tower(mm)			
Length	Radius of down conductor	Top radius	Bottom radius	Height	Average thickness
1250	0.8	88	120	1750	1.2

TABLE 4. Calculated and measured circuit parameters.

Name	Parameters	Measurement	Calculation
Tower	L_t	2.1μH	2.274μH
	C_t	37pF	36.2pF
Down conductor inside blade	L_b	1.1μH/m	0.943μH/m
	C_b	—	9.8pF

The capacitance C_{tm} of segment m is calculated as

$$C_{tm} = \frac{2\pi\varepsilon_0 h_{tm}}{\ln\frac{2h_{tm}}{D_t} - D_m} \tag{11}$$

where h_{tm} ($h_{tm} = h_t/n$) is the length of segment m, h_t is the height of tower, D_t is the equivalent outer diameter of tower, $\varepsilon_0 = 8.85 \times 10^{-12}$F/m. D_m can be evaluated by [14].

The inductance L_{tm} of segment m is calculated as [18]

$$L_{tm} = \frac{\mu_0 h_{tm}}{2\pi}\left(\ln\frac{2h_{tm}}{r_t} - 1 - \mu_r \ln c\right) \tag{12}$$

where μ_r is the relative permeability of tower material [5], $\mu_0 = 4\pi \times 10^{-7}$H/m, $c = r_{in}/r_{out} = (r_t – w)/r_t$ (r_{in} and r_{out} are inner and outer radiuses of the tower, w is the average thickness of the tower and $w \approx r_t/100$).

With each segment represented by a Γ-circuit, the chain-type equivalent circuit is can be obtained for the tower, as shown in Fig. 7.

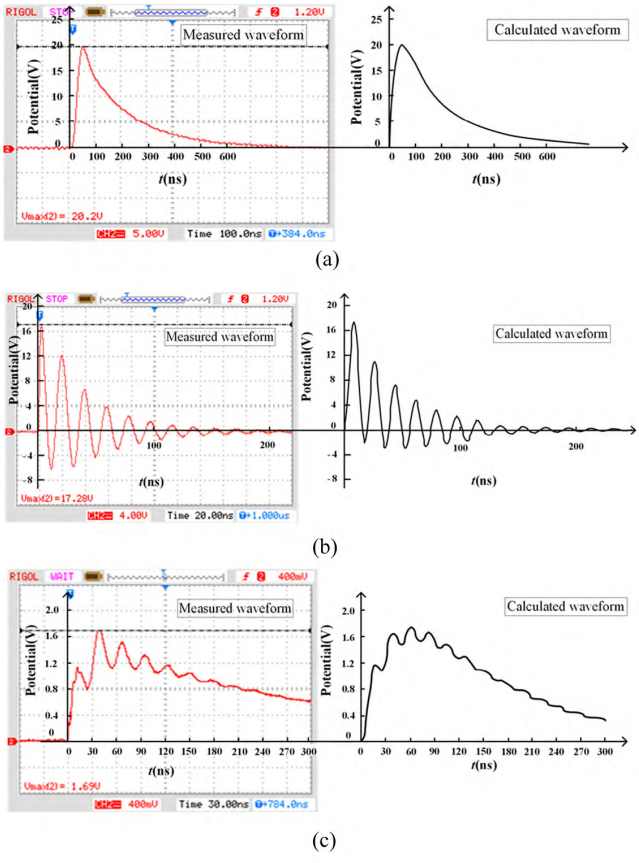

FIGURE 17. Measured and calculated potential waveforms in reduce-scale WT. (a) Across R_n, (b) At the top of tower, (c) At the bottom of tower.

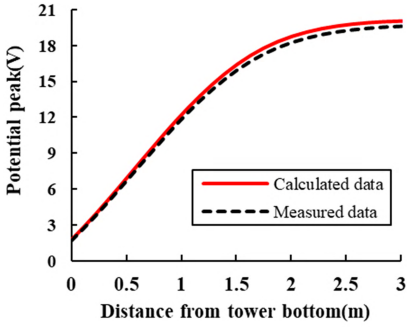

FIGURE 18. Measured and calculated potential distribution along tower.

TABLE 5. Dimensions of an actual WT.

Blade(m)		Tower(m)			
Length	Radius of down conductor	Top radius	Bottom radius	Height	Average thickness
50	4.7×10^{-3}	3.52	4.8	70	4.6×10^{-2}

2) THREE-PHASE CABLE

When a WT is struck by lightning, the lightning current traveling along the tower will induce the overvoltage on the three-phase cable by the electromagnetic coupling effect and do damage to the electric equipment connected to the cable terminals. The three-phase cable inside the tower and its cross-sectional dimension are illustrated in Fig. 8. In a similar manner to the segmentation for the tower, the three-phase cable can also be approximately dissected into a number of segments.

For an arbitrary segment m ($m = 1, 2 \ldots n$), the shielding layer resistance R_1 and cable core resistance R_2 can be calculated [21].The capacitance C_0 between tower and three-phase cable is calculated as [22]

$$C_0 = \frac{2\pi\varepsilon_0 h_{tm}}{\cosh^{-1}\left(\frac{r_t^2+r_3^2-d_{12}}{2r_t r_3}\right)} \tag{13}$$

where $h_{tm} = h_t/n$ (h_t is the height of tower), r_t is the equivalent outer radius of tower, and d_{12} is the distance between the tower and three-phase cable. The capacitance C_1 between shielding layer and cable core is calculated as

$$C_1 = \frac{0.02413\varepsilon_0\varepsilon_r h_{tm}}{\lg\left(\frac{D_{23}}{r_1}\right)} \tag{14}$$

where D_{23} is the distance between the shielding layer and cable core, $\varepsilon_r \approx 6\sim7$. The capacitance C_2 between two cable cores is calculated as

$$C_2 = \frac{\pi\varepsilon_0\varepsilon_r h_{tm}}{\ln\left(\frac{S+\sqrt{S^2-4r_1^2}}{2r_1}\right)} \tag{15}$$

where S is the distance between two cable cores. The inductance per unit length of shielding layer L_1 is 1.4μH [22].The inductance per unit length of cable core L_2 is calculated as

$$L_2 = \frac{\mu_0 h_{tm}}{2\pi}\left(\ln\frac{r_2}{0.7788 r_1}\right) \tag{16}$$

On the basis of the calculated inductances and capacitances, the associated equivalent circuit of cable core and cable shielding layer is given in Fig. 9.

D. MONOPILE FOUNDATION

Offshore WTs with monopile foundation (see Fig. 10) are about 5∼10km away from the shoreline on Chinese offshore wind farms. The offshore WT capacity is typically 1.5∼5.0MW and the seawater depth is less than 15m [23]–[25]. The current dissipating performance of the monopile foundation is characterized by the grounding resistance. The lumped grounding resistance is used for transient calculation.

Fig. 11 shows the curve of grounding resistance R_g varying with the seawater depth h [26], and the curve is obtained from the CDEGS calculation. In [26], grounding resistance R_g is taken as the typical values of 0.2∼0.3Ω, and it can be simplified as several parallel resistors, as shown in Fig. 12. The calculated result further reveals that the value of grounding resistance tends to be invariant after the seawater reaches a depth more than 10m.

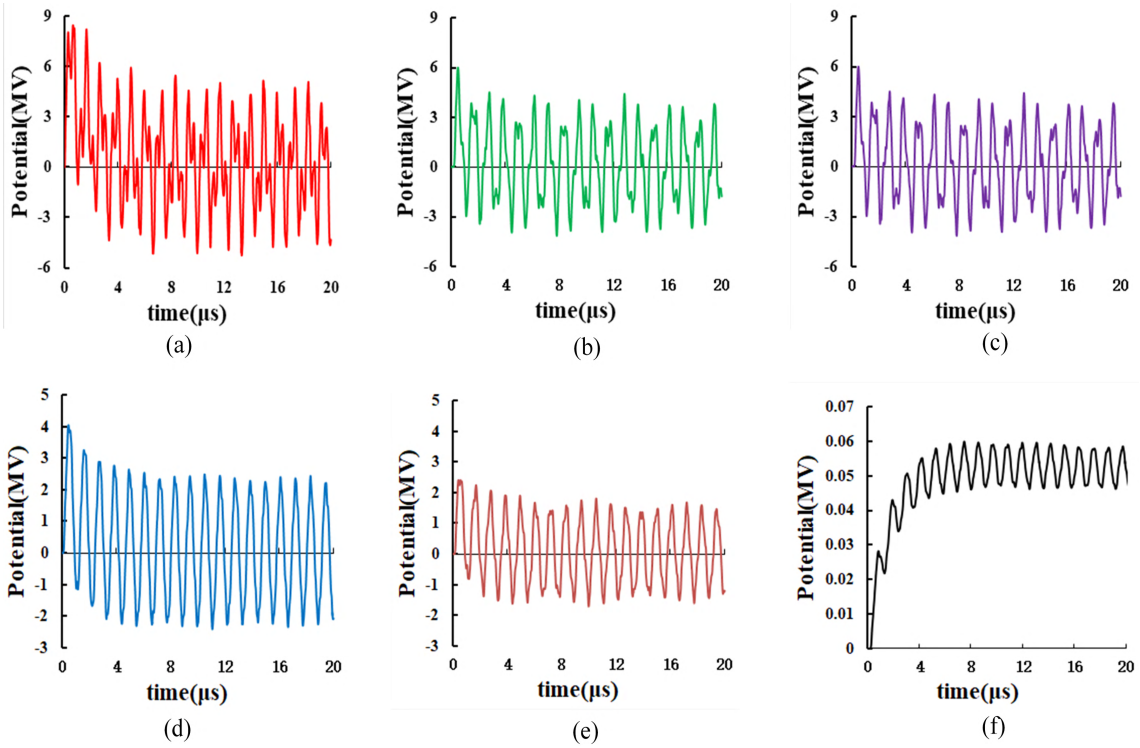

FIGURE 19. Transient potential waveforms under lightning strike to single blade (the striking point is the tip of blade A, the peak value of the injected lightning current is 200kA). (a) At the tip of blade A, (b) At the tip of blade B, (c) At the tip of blade C, (d) At the top of tower, (e) At the middle of tower, (f) At the bottom of tower.

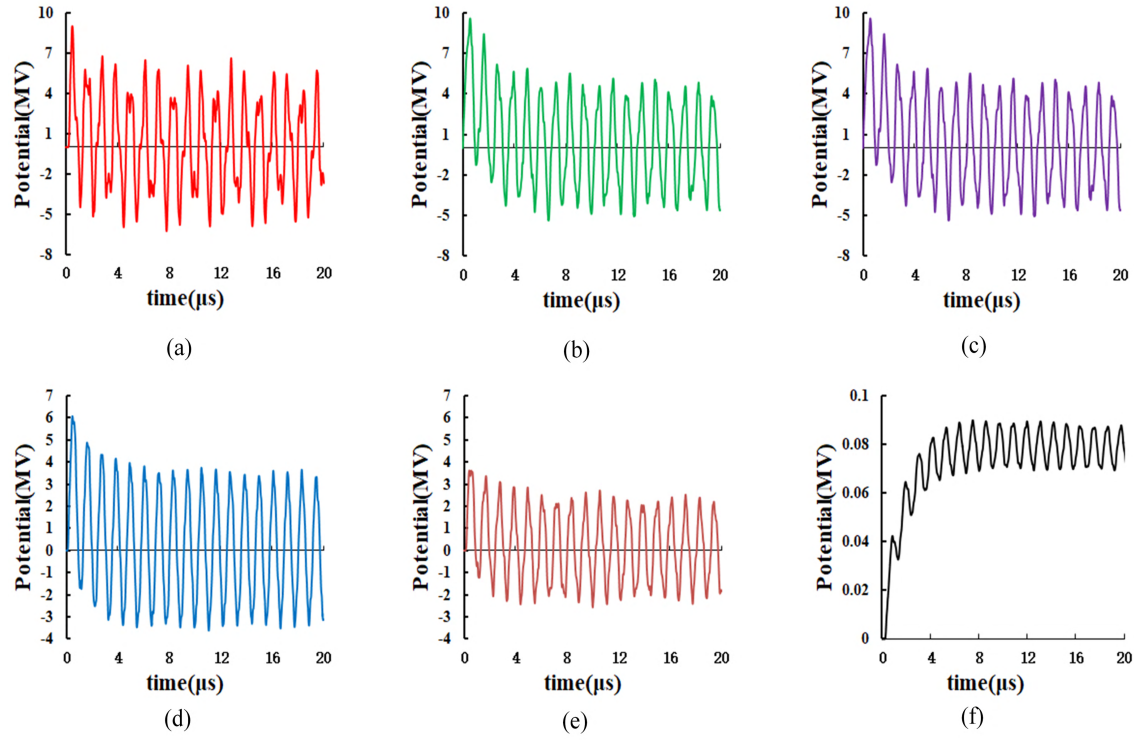

FIGURE 20. Transient potential waveforms under lightning strike to two blades (the striking points are the tips of blades B and C, both peak values of the injected lightning currents are 150kA). (a) At the tip of blade A, (b) At the tip of blade B, (c) At the tip of blade C, (d) At the top of tower, (e) At the middle of tower, (f) At the bottom of tower.

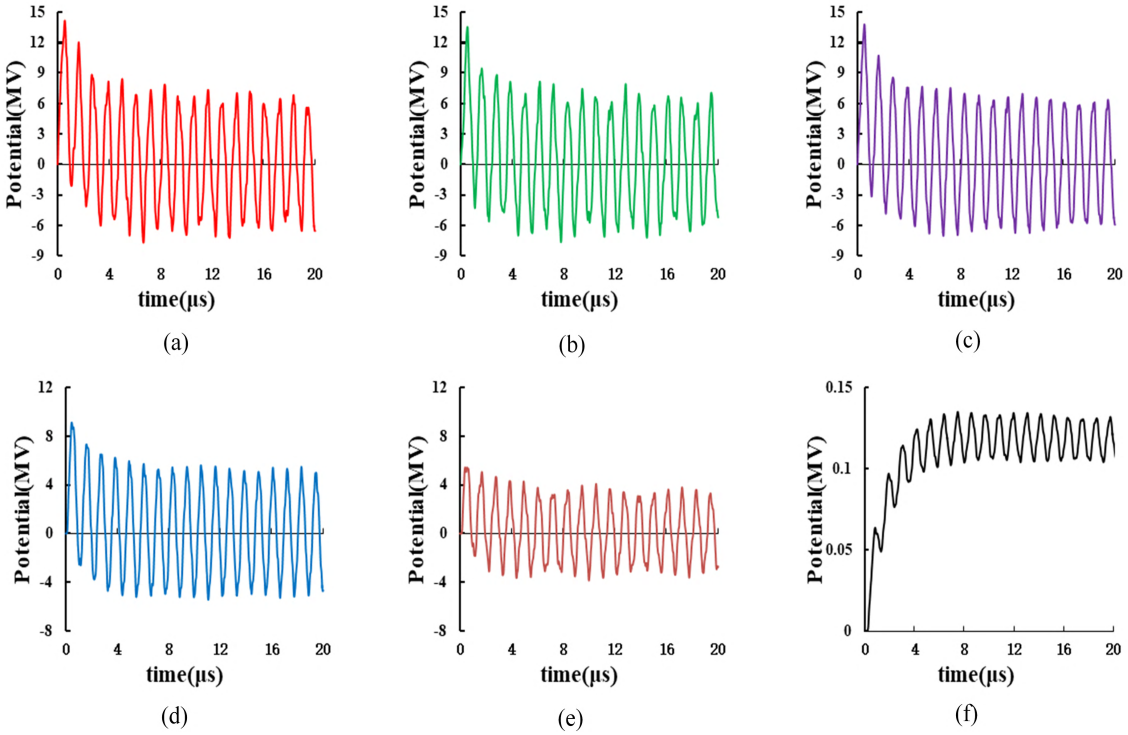

FIGURE 21. Transient potential waveforms under lightning strike to three blades (the striking points are the tips of blades A, C and B, the three peak values of the injected lightning currents are 200kA, 150kA and 100kA, respectively). (a) At the tip of blade A, (b) At the tip of blade B, (c) At the tip of blade C, (d) At the top of tower, (e) At the middle of tower, (f) At the bottom of tower.

E. THREE CASES OF LIGHTNING STRIKE TO BLADES

In view of the actual possibility of lightning strike to the blades [4], the three cases are considered in the transient calculation. Fig. 13 shows a damage event in Chinese wind form, where the three blades are simultaneously damaged by lightning strike. The lightning strike to a blade is modeled as a current source injecting to the blade tip, as shown in Fig. 14.

The information on the mechanism of lightning strike to multi-blade is rare at present, so two kinds of the current injection modes [7], [27] are considered to obtain the transient responses under the lightning current waveforms +10/350μs and $-1/200\mu$s, as shown in Tab 2.

After integrating the five separate equivalent circuits described above and taking into account the three cases of lightning strike to blades, a complete equivalent circuit model is built for a WT under lightning strike to multi-blade, as shown in Fig. 15. Thus, the lightning transient responses can be obtained at different locations on the WT by performing the transient calculation for the circuit model.

III. EXPERIMENTAL VERIFICATION

Fig. 16 shows the experimental arrangement [28], where R_n is non-inductive resistor for current measurement. The impulse current with steep wavefront produced by an impulse generator is injected to the blade tip of the reduced-scale WT. The lead wire for measuring the transient potential is spatially perpendicular to the current lead wire to restrain the electromagnetic induction between them and connected to the grounded steel plate. The current and potential signals are recorded by a digital oscilloscope. As the blade in the vertical position is easily striked by lightning, other rotation positions at different deflection angles are not considered in the experiment for the sake of simplicity.

The dimensions of the blades and tower in experimental arrangement are given Tab. 3. The measured and calculated circuit parameters of the blade and tower are given in Tab. 4, and an approximate agreement between them confirms the validity of the calculating method of the circuit parameters. In order to check the validity of the circuit model of the WT, a few measured and calculated potential waveforms are shown in Fig. 17.

A contrast between them shows that they are relatively close to each other in the peak values, oscillation periods and damping tendency. The measured and calculated potential peak values along the experimental model of the WT are also shown in Fig. 18. As can be seen from Figs. 17-18, the measured results are roughly consistent with the calculated ones, which confirm the validity of the circuit model of the WT.

IV. NUMERICAL EXAMPLE

The dimensions of an actual Chinese-built offshore WT are given Tab. 5. The grounding resistance is taken as $R_g = 0.272\Omega$, which is a typical value at a seawater depth more than 10m. The transient potentials at different locations on the offshore WT are obtained from the circuit model proposed above.

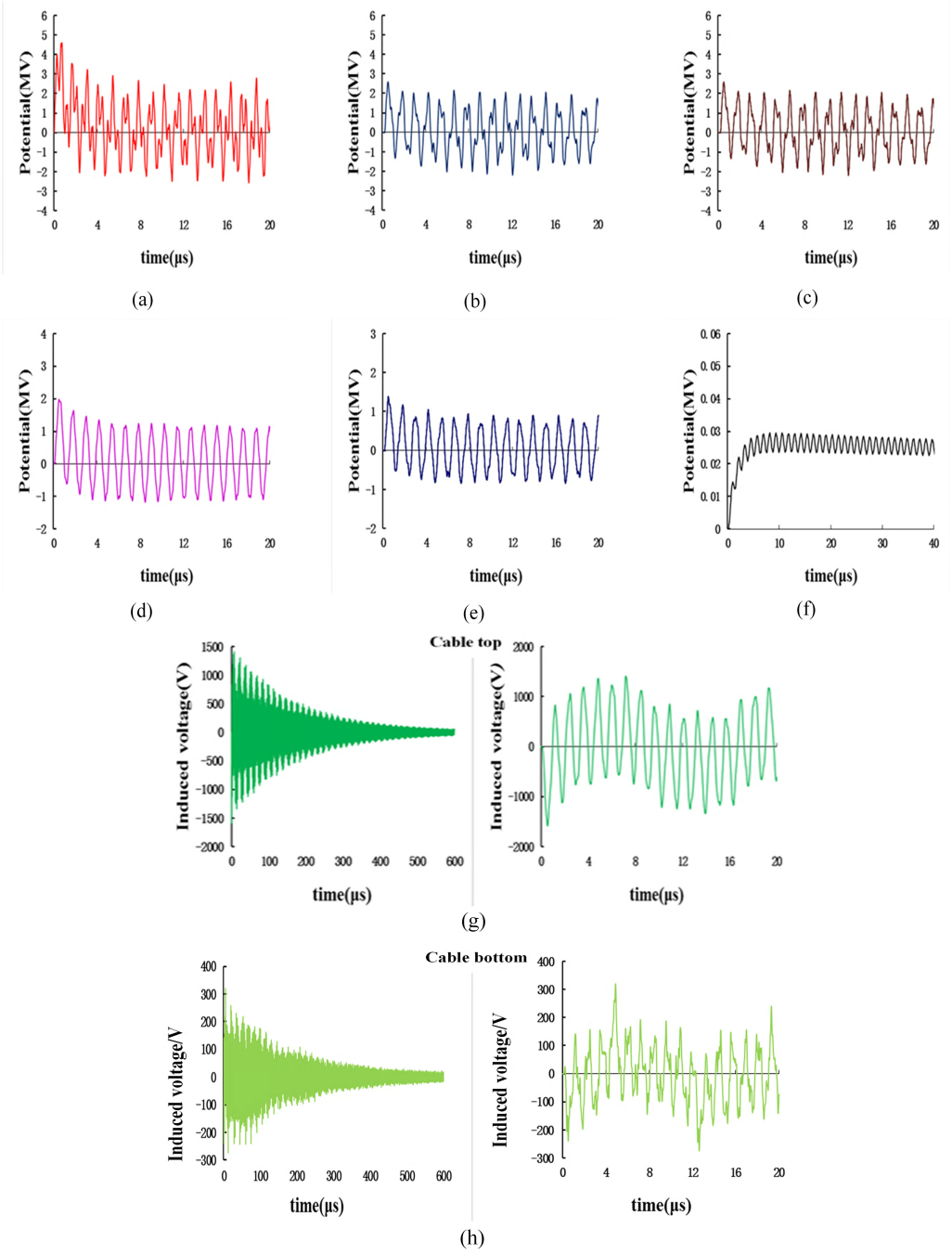

FIGURE 22. Transient potential waveforms under lightning strike to single blade (the striking point is the tip of blade A, the peak value of the injected lightning current is 100kA). (a) At the tip of blade A, (b) At the tip of blade B, (c) At the tip of blade C, (d) At the top of tower, (e) At the middle of tower, (f) At the bottom of tower, (g) At the top of cable, (h) At the bottom of cable.

A. TRANSIENT POTENTIAL WAVEFORMS UNDER +10/350μs LIGHTNING CURRENT

Figs. 19-21 show the transient potential waveforms at a few typical location on the WT under lightning strike to single, two, and three blades (see Fig. 14), where the peak values of the injected lightning currents are taken as 200kA, 150kA, and 100kA, respectively.

As can be seen from the potential waveforms shown in Figs. 19-21, the transient potentials on blade and tower increase with the number of the blades struck by lightning. The reason for this phenomenon is that lightning currents flowing together to the blade root and tower become higher as the number of blades struck by lightning increases. The current convergence causes the potential level at the

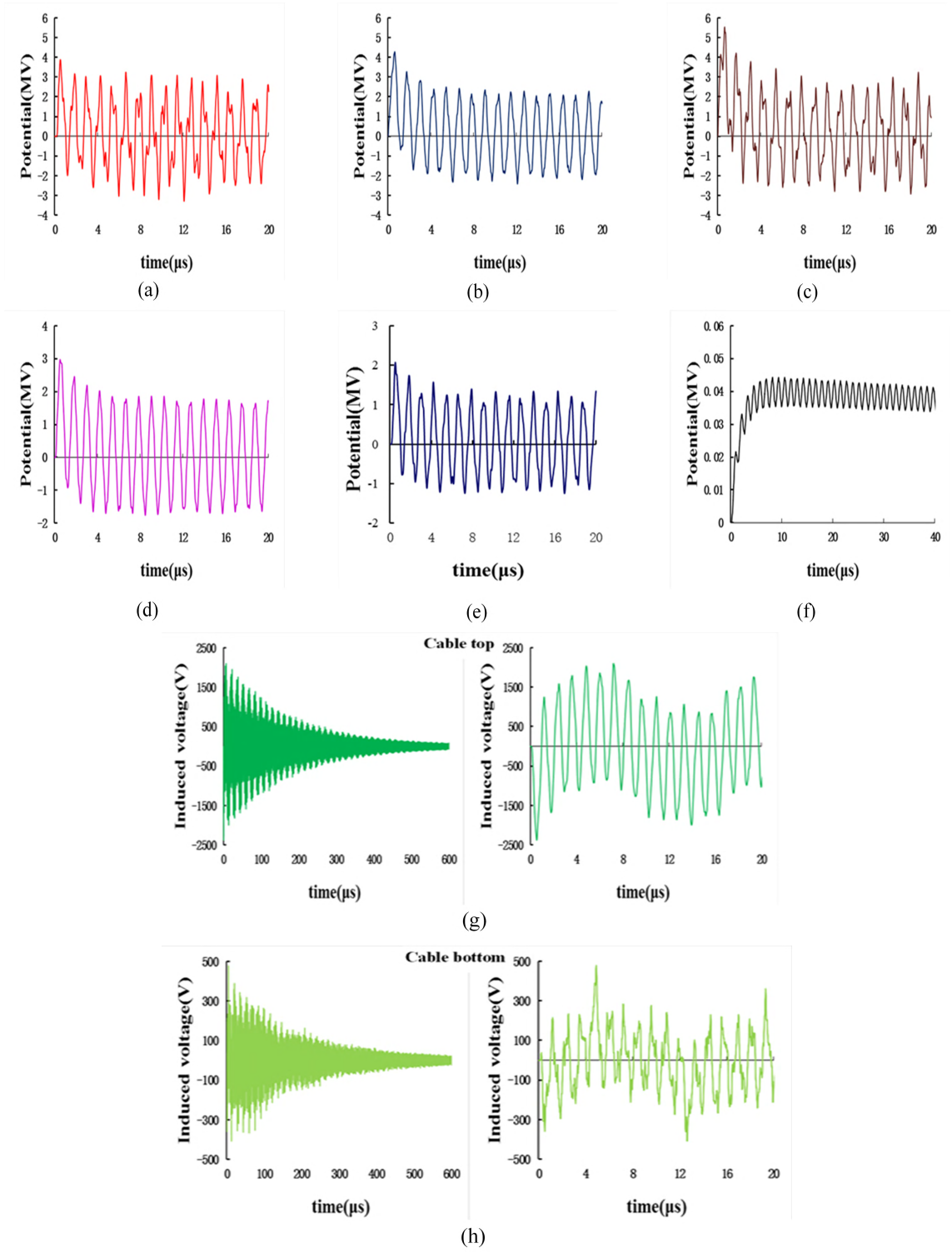

FIGURE 23. Transient potential waveforms under lightning strike to two blades (the striking points are the tips of blades B and C, both peak values of the injected lightning currents are 100kA). (a) At the tip of blade A, (b) At the tip of blade B, (c) At the tip of blade C, (d) At the top of tower, (e) At the middle of tower, (f) At the bottom of tower, (g) At the top of cable, (h) At the bottom of cable.

blade root junction and tower to rise. On this basis, further potential rise will occur at the blade tips. In addition, the potential waveforms exhibit obvious oscillating behavior. This behavior directly results from the inductances and capacitances in the circuit model. It also indirectly embodies the reflection and refraction effects of the traveling waves.

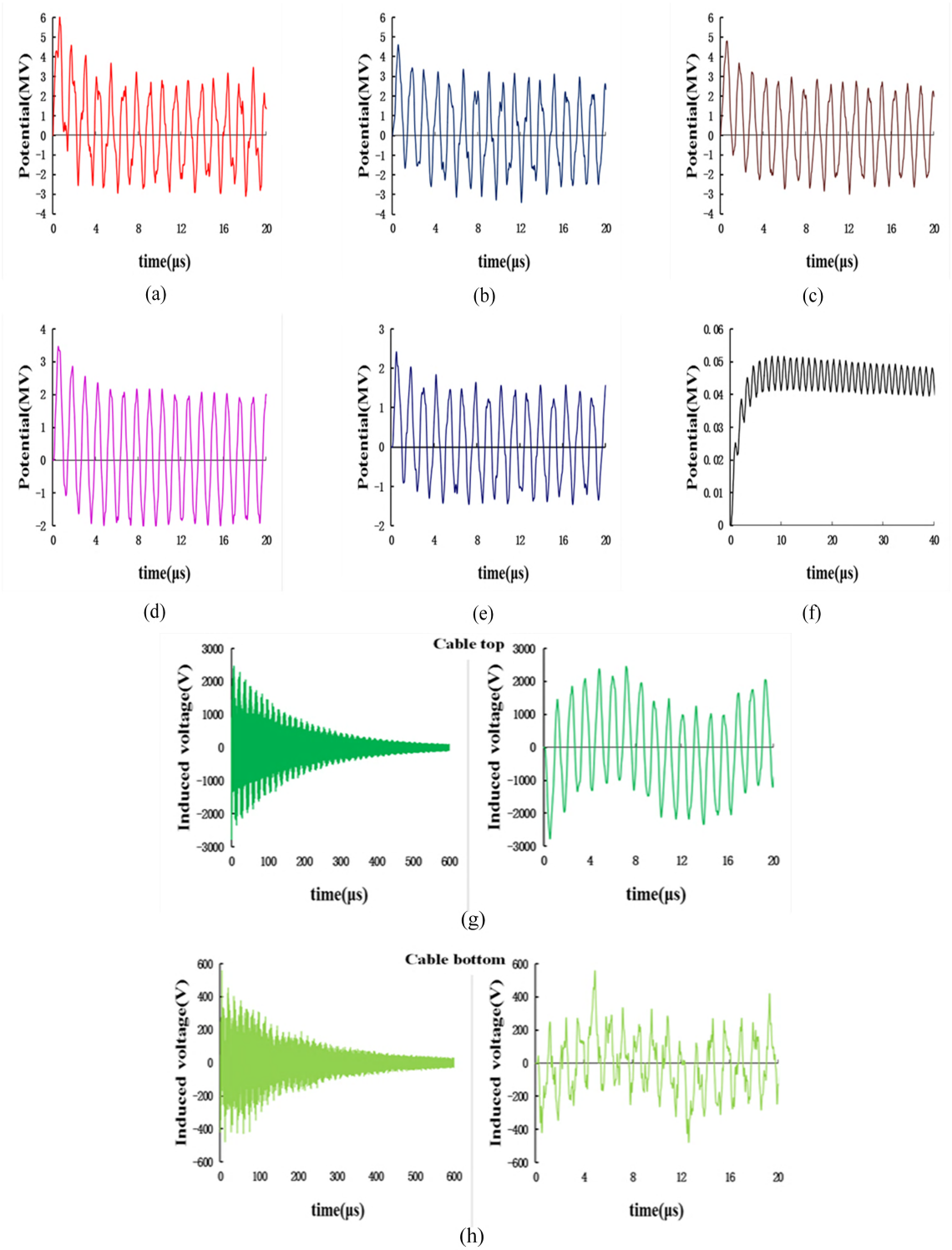

FIGURE 24. Transient potential waveforms under lightning strike to three blades (the striking points are the tips of blades A, C and B, the three peak values of the injected lightning currents are 100kA). (a) At the tip of blade A, (b) At the tip of blade B, (c) At the tip of blade C, (d) At the top of tower, (e) At the middle of tower, (f) At the bottom of tower, (g) At the top of cable, (h) At the bottom of cable.

In fact, determination of the transient potentials on the blade is essential for the lightning protection design of the blade. In terms of the potential difference between two specified points on the blade, the potential gradient can be estimated. Subsequently, the situation of creeping discharge on the blade can be further assessed. As a number of receptors are usually installed on the blade of multi-megawatt WT, a reasonable distance between the two receptors needs to be

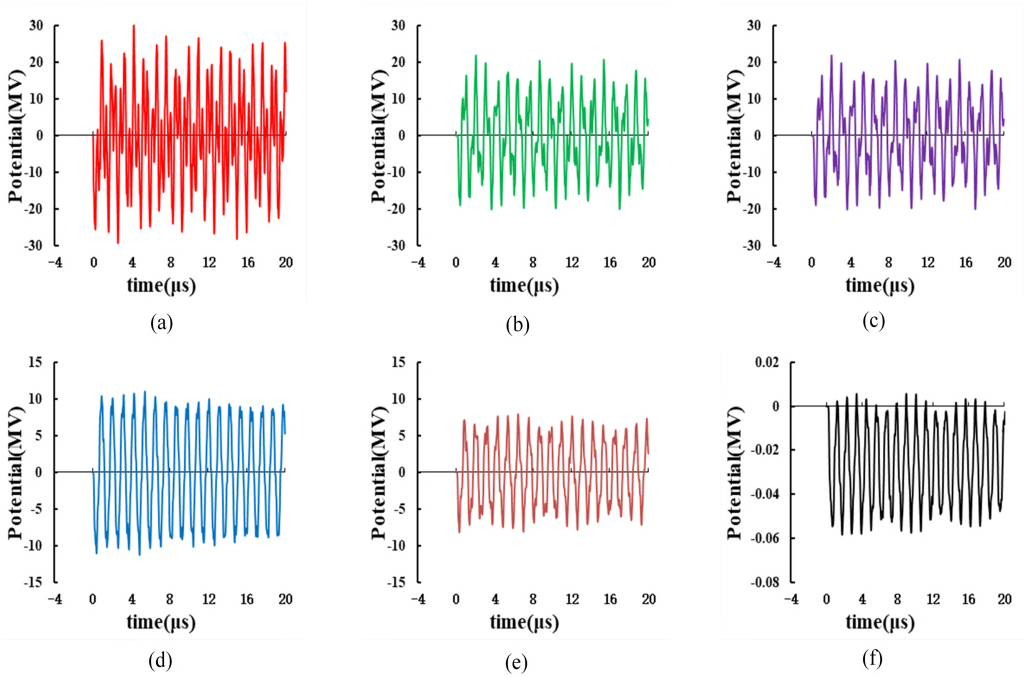

FIGURE 25. Transient potential waveforms under lightning strike to single blade (the striking point is the tip of blade A, the peak value of the injected lightning current is −100kA). (a) At the tip of blade A, (b) At the tip of blade B, (c) At the tip of blade C, (d) At the top of tower, (e) At the middle of tower, (f) At the bottom of tower.

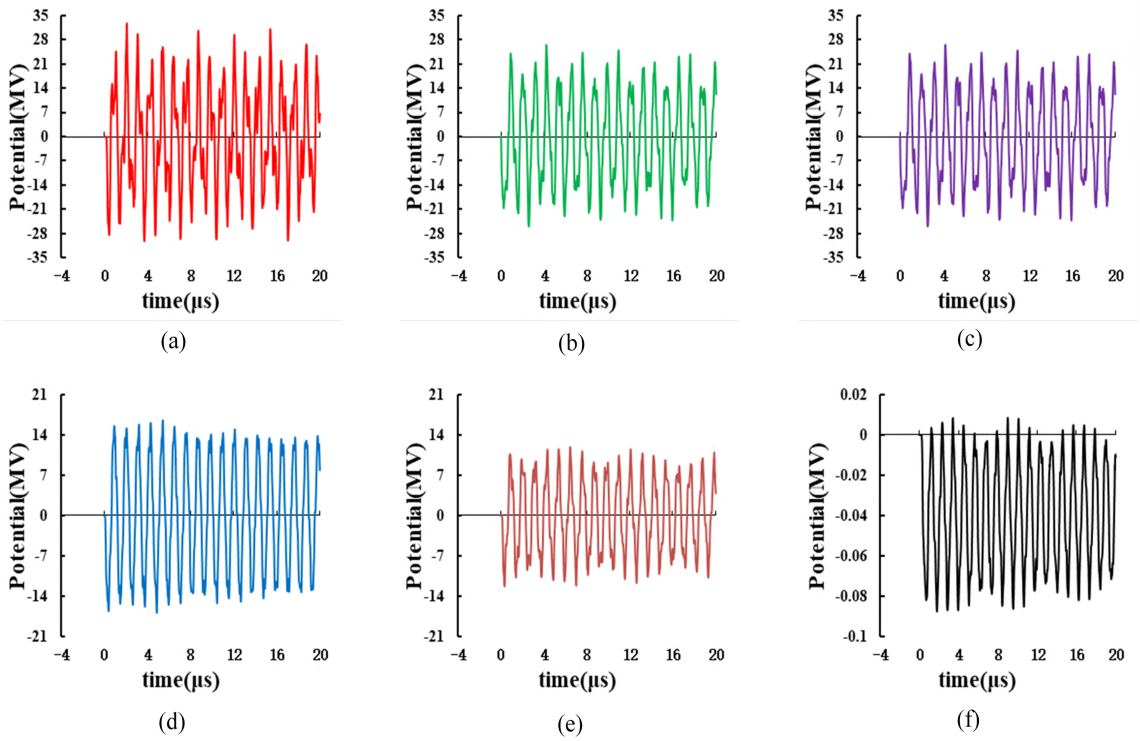

FIGURE 26. Transient potential waveforms under lightning strike to two blades (the striking points are the tips of blades B and C, both peak values of the injected lightning currents are −75kA). (a) At the tip of blade A, (b) At the tip of blade B, (c) At the tip of blade C, (d) At the top of tower, (e) At the middle of tower, (f) At the bottom of tower.

chosen to avoid the creeping discharge and thermal damage to the blade material, which depends to a large degree to knowledge of the transient potential distribution on the blade. At the same time, the high transient potentials on the tower are liable to cause backflash to the facilities inside the tower during a lightning strike. Based on the potential distribution along the tower, the safe distance can be evaluated for installation of the facilities inside the tower.

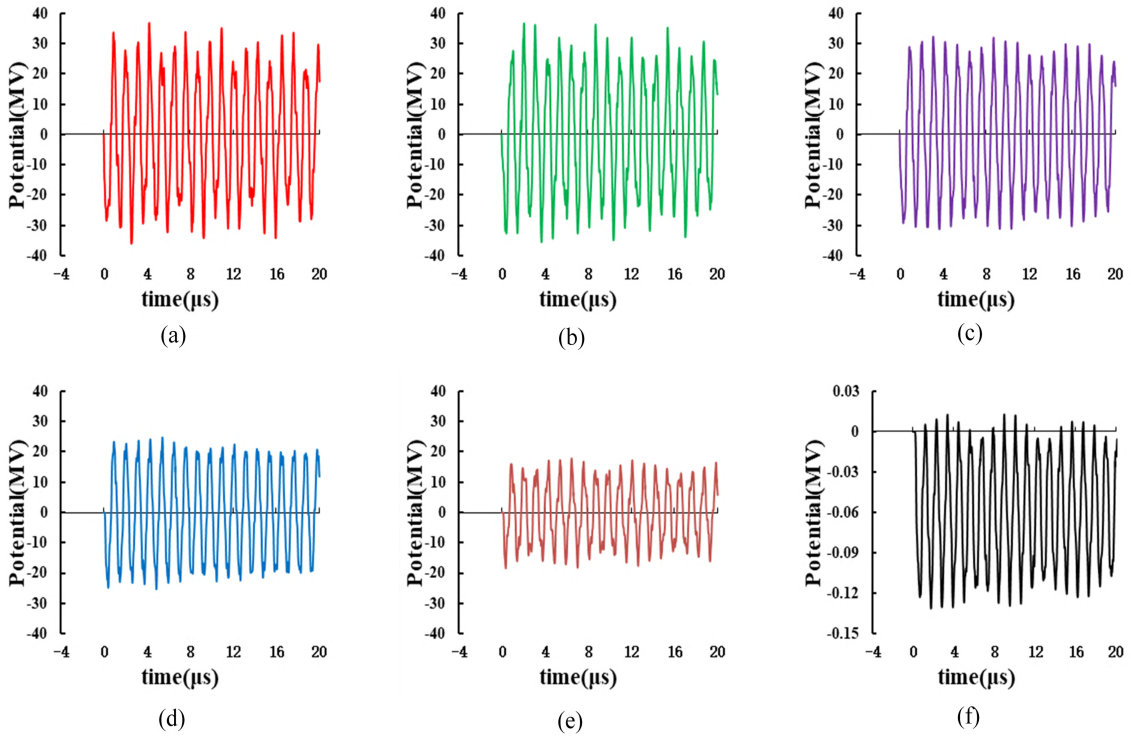

FIGURE 27. Transient potential waveforms under lightning strike to three blades (the striking points are the tips of blades A, C and B, the three peak values of the injected lightning currents are −100kA, −75kA and −50kA, respectively). (a) At the tip of blade A, (b) At the tip of blade B, (c) At the tip of blade C, (d) At the top of tower, (e) At the middle of tower, (f) At the bottom of tower.

As the peak values of the injected lightning currents are concerned, the unequal peak values are considered for the sake of comparison with the case of equal peak value. The lightning current peak values of $+10/350\mu$s are uniformly taken as 100kA, and the transient potential waveforms under lightning strike to multi-blade are shown in Figs. 22-24. The induced voltages between the cable core and shielding layer are also given in Figs. 22-24, where each induced voltage is depicted by two waveforms which have long and short time scales, respectively, for providing a more perfect description for the induced voltages.

In Figs. 22-24, the growth tendency of transient potentials on blade and tower is the same as Figs. 19-21; however, the peak values of transient potentials in Figs. 22-24 are smaller than those in Figs. 19-21. It is evident that the potential peak values are strongly dependent on the sum of injected currents.

At the same time, the transient voltages induced at the cable terminals increase with the number of blades struck by lightning. The induced voltages with thousands of volts will damage the electrical equipment connected at the cable terminals. Therefore, the protection measures need to be taken for protecting against the induced voltages.

B. TRANSIENT POTENTIAL WAVEFORMS UNDER $-1/200\mu$s LIGHTNING CURRENT

When the peak values of the injected lightning currents are taken as −100kA, −75kA, and −50kA, the transient potential waveforms can be shown in Figs. 25-27.

As indicated in Figs. 25-27, the transient potentials increase significantly with the number of the blades struck by lightning. The oscillating behavior under the negative lightning current ($-1/200\mu$s) is stronger than those under the positive lightning current ($+10/350\mu$s); moreover, the potential peak values of the former are higher than those of the latter. The phenomenon is caused by the wavefront time of lightning currents. The shorter the wave front time is, the higher the peak value of transient potential becomes. So the influence of the different lightning current wavefront time needs be considered in the lightning protection design.

V. CONCLUSIONS

A complete circuit model has been proposed for analyzing the lightning transient of the offshore WT in the case of lightning strike to multi-blade. The circuit model gives an overall description to the lightning current path from the tips of blades to the monopile foundation. Using the circuit model to perform transient calculation, the transient responses can be obtained at different locations on the offshore WT. The validity of the model as well as the relevant algorithm of circuit parameters has been verified by the experimental measurement and a good agreement appears between measured and calculated results. To examine the practical feasibility of the circuit model, a numerical example has been given for an actual offshore WT. The lightning strike to multi-blade is investigated in the numerical example. It is found that the transient potential rise on the offshore WT and induced

overvoltages at cable terminals are serious enough to do harm for the facilities and equipment of the offshore WT. Meanwhile, a shorter lightning current wavefront time will cause a sharper transient potential rise. Therefore, some special considerations need to be given to the lightning protection design of offshore WTs.

REFERENCES

[1] N. Malcolm and R. Aggarwal, "Analysis of transient overvoltage phenomena due to direct lightning strikes on wind turbine blade," in *Proc. IEEE Power Energy Soc. General Meeting*, Jul. 2014, pp. 1–5.

[2] *Wind Turbine Generator Systems—Part 24: Lightning Protection*, document IEC 61400-24, 2010.

[3] L. Qian *et al.*, "Analysis of faults and lightning damage of wind power equipment of Dongfang wind farm second stage in Hainan province," *Wind Power*, vol. 66, no. 3, pp. 22–27, 2002.

[4] A. C. Garolera, S. F. Madsen, M. Nissim, J. D. Myers, and J. Holboell, "Lightning damage to wind turbine blades from wind farms in the U.S.," *IEEE Trans. Power Del.*, vol. 31, no. 3, pp. 1043–1049, Jun. 2016.

[5] X. Xiao, *Study on Lightning Overvoltage Protection of Wind Turbines*. Beijing, China: Beijing Jiaotong Univ., 2016.

[6] X.-H. Wang and X.-Q. Zhang, "Modelling and simulation of lightning transients in wind turbine grounding systems," *J. Syst. Simul.*, vol. 22, no. 8, pp. 1805–1808, 2010.

[7] *Wind Turbine Generator Systems—Lightning Protection*, document GB/T 33629-2017, People's Republic of China, Beijing, China, 2017.

[8] F. Rachidi *et al.*, "A review of current issues in lightning protection of new-generation wind-turbine blades," *IEEE Trans. Ind. Electron.*, vol. 55, no. 6, pp. 2489–2496, Jun. 2008.

[9] R. B. Standler, *Protection of Electronic Circuits From Overvoltages*. New York, NY, USA: Wiley, 1989, pp. 68–69.

[10] X. Zhang, "A circuit approach to the calculation of lightning transients in cage-like multiconductor systems," *Int. J. Electr. Eng. Edu.*, vol. 47, no. 2, pp. 213–222, Apr. 2010.

[11] V. A. Rakov *et al.*, "CIGRE technical brochure on lightning parameters for engineering applications," in *Proc. Int. Symp. Lightning Protection (XII SIPDA)*, Belo Horizonte, Brazil, Oct. 2013, pp. 373–377.

[12] S. Mohajeryami and M. Doostan, "Including surge arresters in the lightning performance analysis of 132kV transmission line," in *Proc. IEEE PES Transmiss. Distrib. Conf. Exhib.*, Dallas, TX, USA, May 2016, pp. 1–5.

[13] S. Cristina and A. Orlandi, "Calculation of the induced effects due to a lightning stroke," *IEE Proc. B-Electr. Power Appl.*, vol. 139, no. 4, pp. 374–379, Jul. 1992.

[14] U. Y. Iosseli, A. S. Kothanof, and M. G. Stlyrski, *Calculation of Capacitances*. Moscow, Russia: Electric Power Press, 1987, pp. 24–30.

[15] Q. Zhou, *Lightning-Induced Impulse Magnetic Fields in High-Rise Buildings*. Hong Kong: Hong Kong Polytechnic Univ., 2007.

[16] J. Heppe, "Computation of potential at surface above an energized grid or other electrode, allowing for non-uniform current distribution," *IEEE Trans. Power App. Syst.*, vol. PAS-98, no. 6, pp. 1978–1989, Nov. 1979.

[17] C. R. Paul, *Inductance: Loop and Partial*. New York, NJ, USA: Wiley, 2010, pp. 236–239.

[18] P. L. Kalantrof and L. A. Ceitlin, *Manual of Inductance Calculation*. Moscow, Russia: Electric Power Press, 1992, pp. 3–10.

[19] C. Buccella and M. Feliziani, "A hybrid model to compute the effects of a direct lightning stroke on three-dimensional structures," *IEEE Trans. Magn.*, vol. 39, no. 3, pp. 1586–1589, May 2003.

[20] H.-X. Zhao and X.-R. Wang, "Overvoltage analysis of wind turbines due to lightning stroke," *Power Syst. Technol.*, vol. 28, no. 4, pp. 27–31, 2004.

[21] W. Mingli and F. Yu, "Numerical calculations of internal impedance of solid and tubular cylindrical conductors under large parameters," *Trans. China Electrotech. Soc.*, vol. 151, no. 1, pp. 67–72, 2004.

[22] L. Jingguang, "Calculation and analysis of several electrical parameters of low voltage power cable," *Wire Cable*, pp. 17–19, 1998.

[23] Y. F. Duan, H. Y. Ran, and L. I. Feng-Li, "Design of foundation for offshore wind field," *J. Water Resour. Archit. Eng.*, vol. 8, no. 1, pp. 129–131, 2010.

[24] Z. N. Zheng *et al.*, "Grounding impedance calculation of steel monopile foundations of offshore wind turbines in intertidal zone," in *Proc. ICLP* Oct. 2014, pp. 946–949.

[25] J. M. Prousalidis, M. P. Philippakou, N. D. Hatziargyriou, and B. C. Papadias, "The effects of ionization in wind turbine grounding modeling," in *Proc. 10th Medit. Electrotech. Conf.*, May 2000, pp. 940–943.

[26] T. Shiqi, X. Zhang, and K. Huang, "A simulation exploration on the grounding characteristic of monopile foundation offshore wind turbines," *J. Renew. Sustain. Energy* vol. 8, no. 6, p. 063304, 2016.

[27] *Design Code for Protection of Structures Against Lightning*, document GB50057-2010, Ministry of Housing and Urban Rural Development of the People's Republic of China, Beijing, China, 2010.

[28] K. Yamamoto, T. Noda, S. Yokoyama, and A. Ametani, "An experimental study of lightning overvoltages in wind turbine generation systems using a reduced-size model," *Electr. Eng. Jpn.*, vol. 158, no. 4, pp. 22–30, 2007.

SHIQI TAO was born in Chaoyang, China, in 1990. He received the B.Sc. degree in electrical engineering from Beijing Jiaotong University, Beijing, China, in 2013, where he is currently pursuing the Ph.D. degree in electrical engineering. His research interests include electromagnetic transients in power systems and lightning protection of wind turbines.

XIAOQING ZHANG received the M.Sc. and Ph.D. degrees in high voltage engineering from Tsinghua University, Beijing, China, in 1985 and 1990, respectively. Since 1993, he has been with the School of Electrical Engineering, Beijing Jiaotong University, where he is currently a Senior Research Fellow. He has authored six books and over 50 articles. His research interests include high voltage insulation, lightning protection, and electromagnetic transient simulation.

YAOWU WANG was born in Inner Mongolia, China, in 1988. He received the B.Sc. degree and the master's degree in electrical engineering from Beijing Jiaotong University in 2010 and 2015, respectively. He is currently engaged in research on the electromagnetic transient simulation and lightning protection design of PV systems.

JUNFENG YANG was born in Wanrong, China, in 1990. He received the B.Sc. degree in electrical engineering from Beijing Jiaotong University, Beijing, China, in 2012, where he is currently pursuing the Ph.D. degree in electrical engineering. His research interests include power electronics and electromagnetic compatibility.